Journal of Geoscience and Environment Protection, 2025, 13(10), 104-120
https://www.scirp.org/journal/gep
ISSN Online: 2327-4344
ISSN Print: 2327-4336

Chitosan-Composite Modified Biochar for Remediation of Polycyclic Aromatic Hydrocarbon Pollution

Han Wang[1], Wanke Chen[1], Heng Wang[1], Meifeng Chen[1], Jing Yuan[2*], Qianfeng Zhang[1*]

[1]Institute of Molecular Engineering and Applied Chemistry, Anhui University of Technology, Ma'anshan, China
[2]School of Architecture and Engineering, Tongling University, Tongling, China
Email: *zhangqf@ahut.edu.cn, *154427@tlu.edu.cn

How to cite this paper: Wang, H., Chen, W. K., Wang, H., Chen, M. F., Yuan, J., & Zhang, Q. F. (2025). Chitosan-Composite Modified Biochar for Remediation of Polycyclic Aromatic Hydrocarbon Pollution. *Journal of Geoscience and Environment Protection, 13,* 104-120.
https://doi.org/10.4236/gep.2025.1310008

Received: September 19, 2025
Accepted: October 25, 2025
Published: October 28, 2025

Abstract

Chitosan was composited with raw biochar in different ratios to prepare CBC series materials. The successful loading of chitosan was manifested in the formation of a microporous-dominated membrane structure and a reduction in the specific surface area of the materials, which was subsequently accompanied by an enhancement in structural ordering and an increase in the abundance of surface functional groups, thereby providing more active sites for subsequent adsorption. A novel material was developed in this study for efficiently remediating polycyclic aromatic hydrocarbon-contaminated soils and aquatic environments by blending biochar with chitosan in varying ratios, providing both theoretical foundations and practical references for green environmental remediation technologies.

Keywords

Soil, Water Remediation, Polycyclic Aromatic Hydrocarbons, Chitosan-Biochar Composite, Adsorption Mechanism

1. Introduction

PAHs are referred to as a class of aromatic hydrocarbons with 2 to 7 benzene rings, and are typical persistent organic pollutants (Persistent Organic Pollutants, POPs) that are widely present in the environment. PAHs are generally presented as white or yellowish flaky crystals at room temperature, and most of the PAHs are insoluble in water. Polycyclic aromatic hydrocarbons are characterized by high melting and boiling points, and their vapor pressure is small. Moreover, with the increase in molecular weight, the melting and boiling points increase, and the vapor pres-

sure decreases. The melting point of naphthalene is set at 80˚C, and its boiling point is set at 218˚C; the melting point of anthracene is set at 216˚C, and its boiling point is set at 340˚C. Most of them are insoluble in water and are easily soluble in most organic solvents (Sun et al. 2021). Accompanied by the acceleration of industrialization and urbanization, a significant growth trend has been shown in the accumulation of PAHs. PAHs are endowed with biotoxicity, genotoxicity, mutagenicity, and carcinogenicity potentials. Not only are the ecosystem's material cycle and energy flow interfered with by them, but they also pose potential threats to human health through pathways such as respiratory exposure and dietary intake. Therefore, systematic remediation of PAHs contamination should be carried out without delay. The environmental behavior of PAHs is closely related to their physicochemical properties. An obvious positive correlation is shown between their octanol-water partition coefficients (logKow) and the number of benzene rings (Jones & Voogt, 1999). Lipid solubility and hydrophobicity are enhanced with the increase in the number of rings, which leads to the exponential decrease in the solubility of PAHs in the aqueous phase as the number of benzene rings increases. The solubility of naphthalene (2 rings) in water at 25˚C is usually recorded as 31.7 mg/L, while the solubility of benzo[a]pyrene (5 rings) is only measured at 0.004~0.012 mg/L. The special mode of transport between environmental media has been formed due to the unique physicochemical properties of PAHs (Du et al., 2021): the soil surface layer is rich in plant roots, humus, and other sources of soil organic matter (Bronner & Goss, 2011), and important roles are played by them in the storage and transformation of PAHs (Sweetman et al., 2005). The seasonal significance is shown in the exchange of PAHs at the soil-gas interface: at low temperatures, gas exchange is slowed down, and PAHs tend to accumulate in the soil; at high temperatures, PAHs are released to the atmosphere. Gaseous PAHs can be adsorbed in large quantities by atmospheric fine particles with a diameter of less than 10 μm through surface adsorption and pore interception, and long-distance migration is carried out by them with the atmosphere. Thus, soil and water bodies are polluted again through rainfall deposition and soil-air interface exchange (Cabrerizo et al., 2009; Akyüz & Çabuk, 2010; Kim et al., 2013). PAH transport transformation in water is characterized by a composite type, and its partition coefficient between sediment and water body is affected by sediment adsorption, sediment kinematic state, and salinity of water body (Yuan et al., 2014; Li et al., 2016): Highly cyclic PAHs are easily adsorbed to sediment organic matter due to their high hydrophobicity, but sediment suspension causes them to be desorbed into water (Zhu et al., 2014); At the mouth of the estuary, the partition coefficient is enhanced by a sudden increase in salinity, and the transport of PAHs to the sedimentary phase is promoted (Tremblay et al., 2005). Meanwhile, photodegradation is undergone by PAHs in sediments (Shang et al., 2015). At the same time, bi-directional migration of PAHs between the water column and the atmosphere is carried out through volatilization and wet/dry deposition. The direction of this migration is determined by Henry's law constant and is controlled

by temperature (Fendinger & Glotfelty, 1990). Thus, a storage and release function similar to that of the soil is possessed by the water column-sediment (Wang et al., 2011), and the spatial, temporal, and regional distribution of PAHs is influenced by this trans-media dynamic equilibrium (Li & Duan, 2015).

Biochar is a porous material rich in carbon and oxygen-containing functional groups, which is produced by the high-temperature pyrolysis of plant and animal biomass. A large amount of biomass in nature can be used as biochar feedstock, and different crystalline and pore structures as well as functional groups, are produced under different modification and pyrolysis conditions (Ahmad et al., 2012; Gai et al., 2014). The raw materials are mainly composed of agricultural and forestry wastes, such as straw, rice husk, and wood chips (Kwapinski et al., 2011), animal manure generated from animal husbandry (Li et al., 2021), and industrial solid waste that is subjected to secondary utilization for the manufacture of engineered biochar (Kwon et al., 2022). Biochar is rich in functional groups generated by the pyrolysis of biomass (Wang et al., 2023). In addition, a large specific surface area and high adsorption capacity are exhibited by the carbon skeleton, through which pollutants in soil and water can be effectively adsorbed and immobilized. Biochar is characterized by low cost, high efficiency, and sustainability, and is thus an environmental remediation material with broad application prospects and research value (Fabbri et al., 2013; Wang & Wang, 2019). The adsorption capacity of biochar for pollutants is affected by a combination of factors such as biomass source, surface functional groups, pyrolysis temperature, and specific surface area (Chen et al., 2012; Ding et al., 2016). The number of surface-loaded functional groups on native biochar is limited, and its pore structure is readily blocked by impurities. Therefore, activation and pore cleaning by acid or alkaline solution are necessary to increase the specific surface area, increase the number of functional groups, and enhance the adsorption capacity for pollutants (Mosleh & Rajabi, 2024). The design of biochar requires taking into account the properties of the modified materials and the characteristics of the target pollutants. In order to improve the removal rate of pollutants, biochar needs to be pretreated through processes such as activation or functionalization modification before being applied to a contaminated site (Lee & Park, 2020). For example, the hydrophobicity of carbon material adsorbents can be improved by grafting fluorine-containing functional groups on the surface of carbon materials (Weissmann et al., 2010). It has been shown that the adsorption performance of alkylation-modified porous biochar, which is prepared using esterification and etherification, for low concentrations of volatile organic compounds (VOCs) in high-humidity environments is such that the alkylation-modified porous biochar possesses a large specific surface area and weak surface polarity. Moreover, the interactions between oxygen-containing functional groups and hydrogen bonding are the key factors that control the adsorption capacity of the biochar for VOCs under humid conditions (Cheng et al., 2022). Corn kernel biochar, which is prepared using corn kernels as the biomass feedstock, is rich in hydroxyl groups and a graphene-layered structure. Un-

der visible light illumination, highly reactive hydroxyl radicals are generated through the interaction of photoinduced electrons with the graphite structure and oxygen, by which methyl orange is degraded (Zhang et al., 2020). It is demonstrated by the above studies that the surface of biochar, after undergoing cleaning and activation, can be further modified by the incorporation of additional composite materials, which is considered an effective strategy for enhancing its adsorption performance toward organic pollutants.

This study utilized wheat straw as a biomass feedstock, which was subjected to high-temperature pyrolysis carbonization in a tube furnace to produce straw biochar. Following ultrasonic treatment, impurities and ash were removed from the biochar surface using dilute HCl and NaOH, yielding the raw biochar (RAW-BC) used in this experiment. Chitosan was blended with the raw biochar at varying ratios to prepare the CBC series materials. The remediation efficacy of RAW-BC and the CBC series biochar was evaluated through adsorption experiments simulating naphthalene-contaminated soil and aquatic environments.

2. Materials

Chitosan (AR), sodium hydroxide (AR), potassium bromide (spectrally pure), epichlorohydrin (AR), anhydrous ethanol (AR), acetic acid (AR), methanol (AR), naphthalene (AR), urea (AR), FeSO4-7H2O, anhydrous sodium sulfate (AR), n-hexane (AR), acetone (AR), 98% concentrated hydrochloric acid (AR) were purchased from Sinopharm Chemical Reagent Co. Ltd.; methanol (HPLC) was purchased from Shanghai McLean Biochemical Technology Co. Ltd.

3. Experimental Procedures and Analytical Methods

3.1. Straw-Based Biochar Carbonization

The pyrolysis carbonization method was used to prepare basic biochar materials in the current experiment. The specific operation process was as follows: firstly, the crop straw was pretreated, and then washed with deionized water, screened for impurities, and dried at 60˚C. The pretreated straw was crushed by an ultra-micro-mill, and then passed through a standard sieve (aperture 300 μm) for particle size grading. The sieved powder was placed in a controlled atmosphere tubular pyrolysis furnace under a nitrogen protective atmosphere (flow rate of 1.5 L/min) for the gradient heating treatment: the temperature was increased to 500˚C at 5˚C/min and then maintained at a constant temperature for 4 h. After cooling, the carbonized product was crushed and sieved for the second time, the ash and impurities were removed, and the product was washed by the cycle of deionized water to neutrality (pH = 7.0 ± 0.2), and then dried at 60˚C for 12 h in the drying oven. After vacuum filtration, the product was dried in an oven at 60˚C for 12 h to obtain the original biochar.

3.2. Activation Treatment of Biochar

A large amount of incompletely pyrolyzed ash, minerals, and organic residues re-

main on the surface of the raw carbonized material, and the presence of these impurities affects the pore structure of the biochar and the bonding sites of the composites, which need to be cleaned by acid and alkali to expand the pore structure and specific surface area to enhance the physical adsorption capacity. The raw biochar was first cleaned by hydrothermal ultrasonic cleaning for 2 h and then dried to initially remove the surface impurities, to establish an ideal surface structure for subsequent activation or loading of other composites, and to make the modifier adhere uniformly. Then, after ultrasonication, the biochar was cleaned and dried alternately by using a dilute HCl solution and a dilute NaOH solution for activation, and the biochar treated by the above process was the raw biochar used in this manuscript (RAW After the above process, the biochar is the raw material used in this paper (RAW-BC).

3.3. Preparation of Chitosan Composite Biochar Material

Take two grams of chitosan and dissolve it in 200 mL of a 1% acetic acid aqueous solution. The solution is heated to 50˚C on a constant temperature oil bath magnetic stirrer and slowly stirred for 1 h. Raw biochar powder is added, followed by another 30 min of stirring and 5 min of ultrasonication to allow the biochar to be fully dispersed in the system. Ten milliliters of epichlorohydrin are added as a cross-linking agent, and a 0.1 M NaOH solution is slowly added to adjust the pH to 11 - 12. Stirring is kept at 60˚C for 6 h. Finally, a small amount of anhydrous ethanol is added to adsorb the excess epichlorohydrin, thereby stopping the reaction. The product is then washed alternately with anhydrous ethanol and 1% dilute acetic acid for 2 times to remove the excess epichlorohydrin and unbound chitosan. Afterward, it is washed repeatedly with deionized water until neutral and filtered to near dryness. The product is dehydrated and dried using a freeze dryer for 48 h, then crushed and sieved again for use. The ratio of chitosan to biochar (1:2, 1:4, and 1:6) is changed, and a total of three groups are named CBC 1:2, CBC 1:4, and CBC 1:6.

3.4. Characterization of Materials

Scanning electron microscopy (SEM) was used to observe the morphology of the biochar and its composites (Tungsten filament SEM, JEM-6510) and to investigate the effect of chitosan on the surface structure of the biochar before and after chitosan composite. Fourier transform infrared spectroscopy (FTIR) (Nicolet-6700 FTIR, Thermo Fisher, USA) was used to investigate the functional groups on the surface of the composites before and after chitosan compositing and at different ratios. The spectral scanning range was set from 500 to 4000 cm^{-1}, and a blank potassium bromide pressed into slices was used as a background value for correction with a resolution of 4 cm^{-1}. The specific surface area and pore volume of the composites were analyzed and determined by Brunauer-Emmett-Teller (BET) (Kubo-X1000 Pore Size and Specific Surface Area Analyzer produced by Beijing Biodevelopment Electronic Technology Co., Ltd.). The samples were pretreated

by degassing and activation for 4 h under vacuum at 100˚C, and then the nitrogen adsorption-desorption isotherms were determined at liquid nitrogen temperature (77 K). The desorption isotherm was determined at liquid nitrogen temperature (77 K), the specific surface area was calculated based on the BET model, and the pore size distribution was analyzed by the BJH method. The XPS of biochar and its composites were tested using an X-ray photoelectron spectroscopy analyzer, Thermo Scientific K-Alpha, manufactured by Thermo Fisher, Inc., with a vacuum of approximately 5×10^{-9} mbar in the analysis chamber. X-ray source: monochromated Al-Ka source (Mono Al-Ka) Energy: 1486.6 eV, Voltage: 12 KV, Beam current: 6 mA, analyzer scanning mode: CAE, instrumental figure of merit: 4.2 eV.

3.5. Source of Test Soil, Physical and Chemical Properties, and Testing Methods

The soil was taken from Jiashan District, Maanshan City, and sampled at a depth of 0 - 20 cm from the surface. After air-drying, gravel, twigs, and other impurities were removed, and the soil was sieved through a 50-mesh sieve. Dissolve 0.05 g of naphthalene in 100 mL of methanol in a 500 mL beaker and mix with 100 g of soil. The soil was sealed from light for 3 d and then placed in a fume hood to accelerate the volatilization of methanol. 400 g of uncontaminated soil was added to the soil in 3 additions and stirred with water to homogenize the soil, and the soil was again sealed from light for 30 d and kept at a water holding capacity of about 60%. Thirty days later, the soil was taken out, i.e., it was the PAH naphthalene-contaminated soil used in the experiments. The content of naphthalene in the soil was determined by HPLC and finally amounted to 10 mg/kg.

3.6. Adsorption Studies

3.6.1. Adsorption Effect of Materials on Polycyclic Aromatic Hydrocarbons in Soil

An indoor simulated incubation method was used to investigate the remediation effects of different materials on naphthalene in contaminated soil. Five groups of parallel experiments were set up, and 150 mL brown glass conical flasks with stoppers were used as the incubation containers. Each group was initially filled with 50 g of contaminated soil with a naphthalene concentration of 10 mg/Kg, and 5 g of different biochar materials were added to each experimental group. All samples were sealed immediately after the addition of biochar, and the sealed flasks were placed in a fume hood and wrapped in a cardboard box for incubation in order to avoid naphthalene degradation by light. Soil samples were taken at five predetermined time points (7, 14, 30, 45, and 60 d). All five culture systems were processed simultaneously at each sampling, and after rapid fixation of the samples with a freeze-dryer, the residual concentrations of naphthalene in the soil were quantified using a Shimadzu high-performance liquid chromatograph (HPLC).

3.6.2. Calculation of PAH Removal Rate

PAH content (mg/kg) in soil samples was calculated according to the formula:

$$\omega_i = \frac{\rho_i \times V}{m \times W_{dm}} \quad (1)$$

where: ω_i is the content of component i in the sample, μg/Kg; ρ_i is the concentration of component i calculated from the standard curve, μg/mL; V is the volume of calibration, mL; m is the weight of the sample (wet weight), Kg; W_{dm} is the content of dry matter in the soil sample, %.

Calculation formula for the PAH removal rate:

$$\eta = \left(\frac{C_0 - C_i}{C_0} \right) \times 100\% \quad (2)$$

where: C_0 is the concentration of naphthalene in the control group, mg/L; C_i is the concentration of naphthalene in the experimental group, mg/L.

3.6.3. Adsorption Mechanism

To simulate the pollution of PAHs in water under natural conditions: 0.1 g of naphthalene was dissolved in a small amount of methanol solution, a small amount of 0.01 M $CaCl_2$ solution was added to provide a certain ionic strength, and then a 100 ml volumetric flask was used for the methanol solution of 1000 mg/L naphthalene, which was used as the background solution, and the background solution was diluted again. A small amount of deionized water was added into a 1 L brown volumetric flask, 10 mL of the background solution was added into the volumetric flask several times, and ultrasonication was performed for 10 min to ensure the pollutant solution mixed well after the deionized water was used to fix the volume, i.e., 10 mg/L of simulated contaminated water was used in this experiment.

3.6.4. Adsorption Kinetic Studies

Pseudo-primary, pseudo-secondary, Elovich, and intraparticle diffusion models were used for kinetic modeling, and Langmuir and Freundlich isotherm models were used to describe adsorption isotherm processes.

The equations used for kinetic modeling are (Wang & Guo, 2020):

Pseudo-first order:

$$\frac{\mathrm{d}q_t}{\mathrm{d}t} = k_1 \left(q_e - q_t \right)$$

Pseudo-second order:

$$\frac{\mathrm{d}q_t}{\mathrm{d}t} = \frac{1}{k_2 q_e^2} + \frac{t}{q_e}$$

Elovich model:

$$q_t = \frac{1}{\alpha} \ln \left(\alpha\beta t + 1 \right)$$

The linearized form is:

$$q_t = \frac{1}{\beta} \ln \left(\alpha\beta \right) + \frac{1}{\beta} \ln t$$

where: q_e is the equilibrium adsorption amount, mg/g; q_t is the adsorption amount at time t, mg/g; k_1 is the pseudo-primary rate constant; k_2 is the pseudo-secondary rate constant; α is the initial adsorption rate constant, mg/g^{-1}·min^{-1}; and β is the desorption constant associated with surface coverage, g/mg.

4. Results

4.1. Characterization of Chitosan-Modified Biochar Materials

As shown in Figure 1, the broad peaks in the range of 3200 to 3600 cm^{-1} correspond to the stretching vibration of hydroxyl groups on the surface of biochar (Luo et al., 2018). All samples showed strong absorption peaks near the aromatic backbone vibration (C = C) at 1630 cm^{-1}, corresponding to the C = C stretching vibration of the graphitized structure of biochar. The peak shape in this region was stable, which indicated that the carbon backbone was structurally intact, which was conducive to the adsorption of polycyclic aromatic hydrocarbons through π-π interaction (Li et al., 2020). The ether bonding and oxygen-containing groups (C – O) were in the range of 1000 - 1300 cm^{-1} (e.g., 1050 cm^{-1}), corresponding to the vibration of C-O-C or phenolic hydroxyl groups, and the increase in peak intensity of CBC 1:2 in this region suggests that the increase in oxygen-containing functional groups enhances the polarity via hydrogen bonding adsorption capacity (Huang et al., 2020).

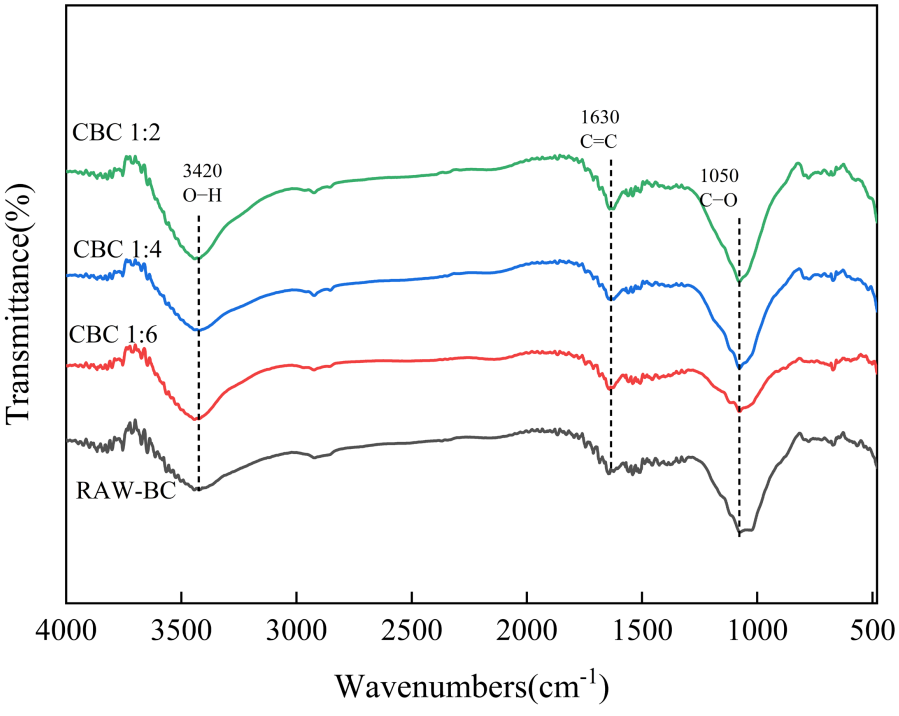

Figure 1. Infrared spectra of RAW-BC and CBC series biochar.

Scanning electron microscopy (SEM) results showed that before compositing, the biochar was a straw-based porous carbon skeleton with only a few impurities

present in the pores (**Figure 2(a)**, **Figure 2(b)**). After compositing, as shown in **Figure 2(c)** and **Figure 2(d)**, chitosan was adhered to the surface of the biochar in the form of thin films or particles, through which the original pores were partially covered. Meanwhile, a 50 - 200 nm nanoscale fold structure was introduced, and the surface roughness was significantly improved. This improvement is related to the formation of a three-dimensional network structure by the entangled cross-linking of chitosan molecular chains (Queiroz et al., 2023). As the mass ratio of chitosan to biochar composite decreases (1:2 → 1:6), the area covered by the chitosan film on the surface of biochar gradually becomes smaller and thinner, and the outer surface structure is exposed (e.g., **Figure 2(e)**, **Figure 2(f)**). Although the original pore size and outer surface structure of the biochar are partially blocked by chitosan, a large number of functional groups are contained in its film, through which the chemisorption performance of PAHs can be enhanced (Buttersack, 2019).

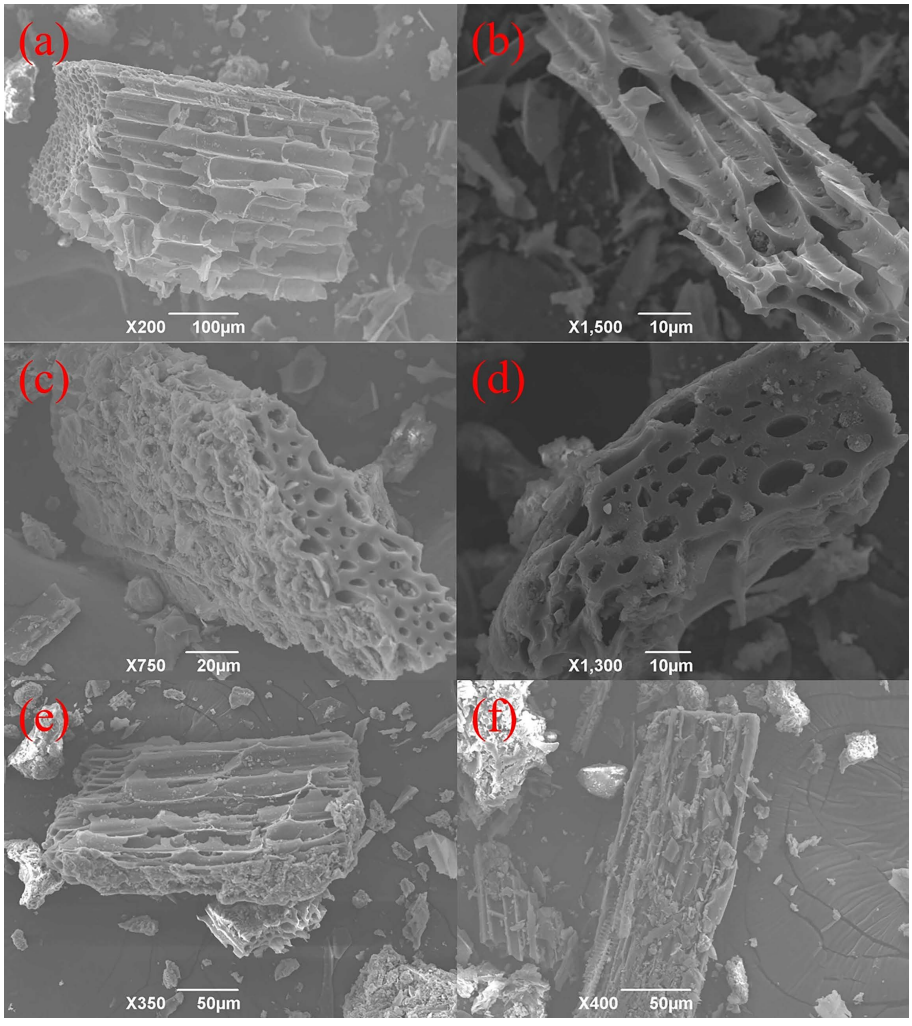

Figure 2. Scanning electron micrographs of RAW-BC and CBC series biochar: (a) (b) RAW-BC surface before modification; (c) CBC 1:2 outer surface; (d) CBC 1:2 pores; (e) CBC 1:4 outer surface; (f) CBC 1:6 outer surface.

According to **Figure 3**, the N_2 adsorption-desorption curves of each biochar material were all type IV adsorption isotherms and had H3 hysteresis loops (Fu et al., 2019), indicating that the biochar has a layered structure and mesopores (Zhang et al., 2022), which is in agreement with the results of scanning electron microscopy. BET results indicate that within the CBC series of biochar, as the composite ratio of chitosan to biochar increased from 1:2 to 1:6, the specific surface area decreased significantly to 6.2294 m^2/g before rebounding to 8.216 m^2/g. This indicates that chitosan promotes the formation of macropores on the biochar surface, where increased pore volume provides more effective adsorption sites (Huang et al., 2022). Total pore volume and pore size significantly expanded, albeit at the expense of specific surface area, rendering the biochar more suitable for macromolecular adsorption scenarios.

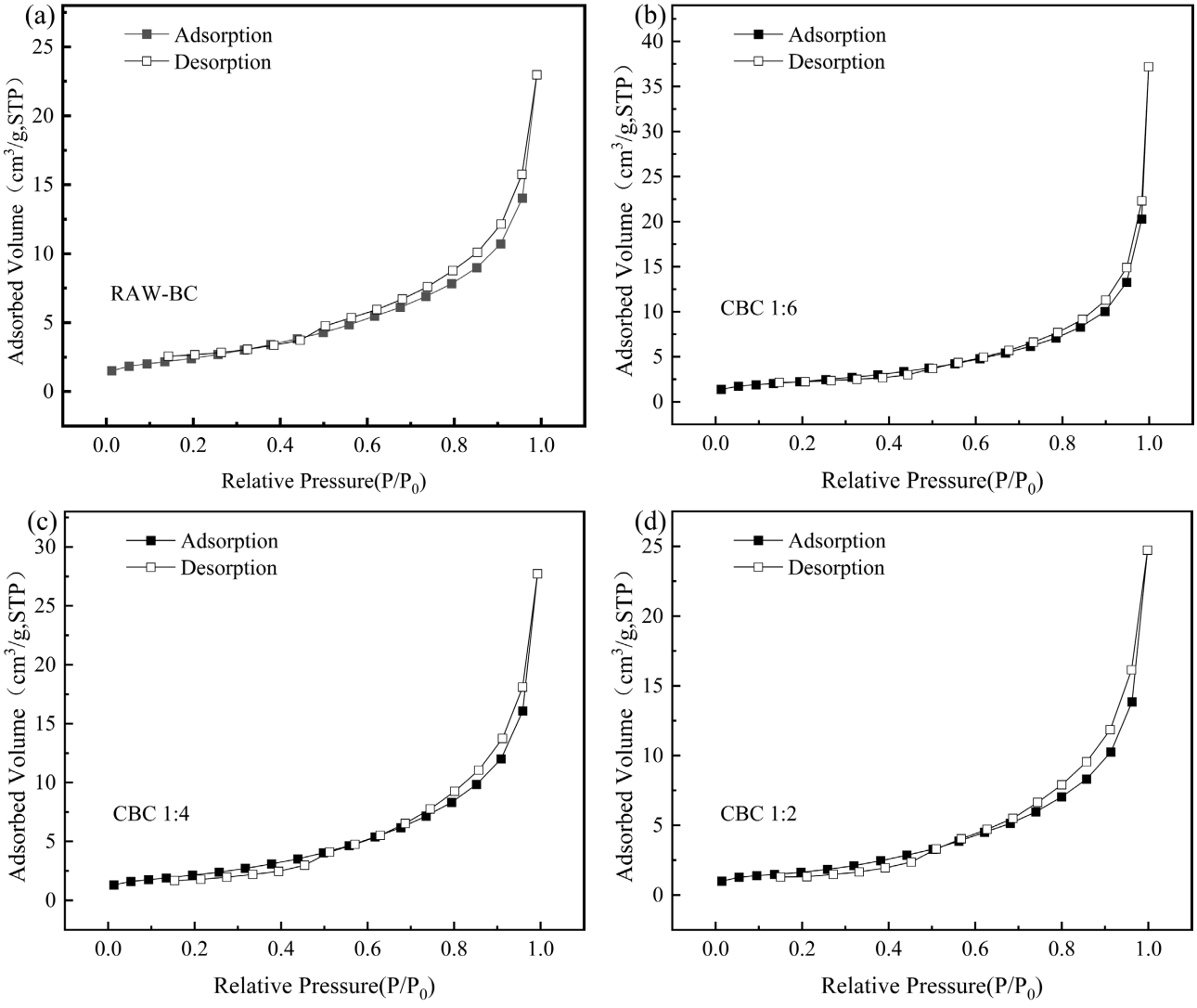

Figure 3. N_2 adsorption-desorption curves of RAW-BC and CBC series biochar: (a) RAW-BC; (b) CBC 1:6; (c) CBC 1:4; (d) CBC 1:2.

XPS spectral analysis (**Figure 4**) shows that the whole spectrum of RAW-BC

contains C1s, O1s, and N1s peaks, with a simple elemental composition. CBC 1:2 has higher C, N, and O elemental contents than RAW-BC. In the C1s spectrum, RAW-BC is dominated by graphitized carbon (283.9 eV, 63.04%), and also contains C=O (288.8 eV), C-C, and C-N (285.0 eV). Meanwhile, CBC 1:2 contains C=O (287.5 eV), C-C (284.8 eV), graphitized carbon (283.6 eV), and C-N (pyridine/pyrrole type, 285.7 eV), suggesting that the carbon structure has been changed by the introduction of nitrogen-containing functional groups from chitosan. In the N1s spectrum, only pyrrole nitrogen (399.3 eV) is contained in RAW-BC, while pyridine nitrogen (398.3 eV) and graphitic nitrogen (401.1 eV) are contained in CBC 1:2. This is a more complex form of nitrogen, through which chemical stability and activity can be enhanced, and the number of reaction sites can be increased. Overall, the nitrogen-containing functional groups of CBC 1:2 have been diversified through modification with chitosan, and its surface chemistry is more complex, which affects its adsorption function for PAHs.

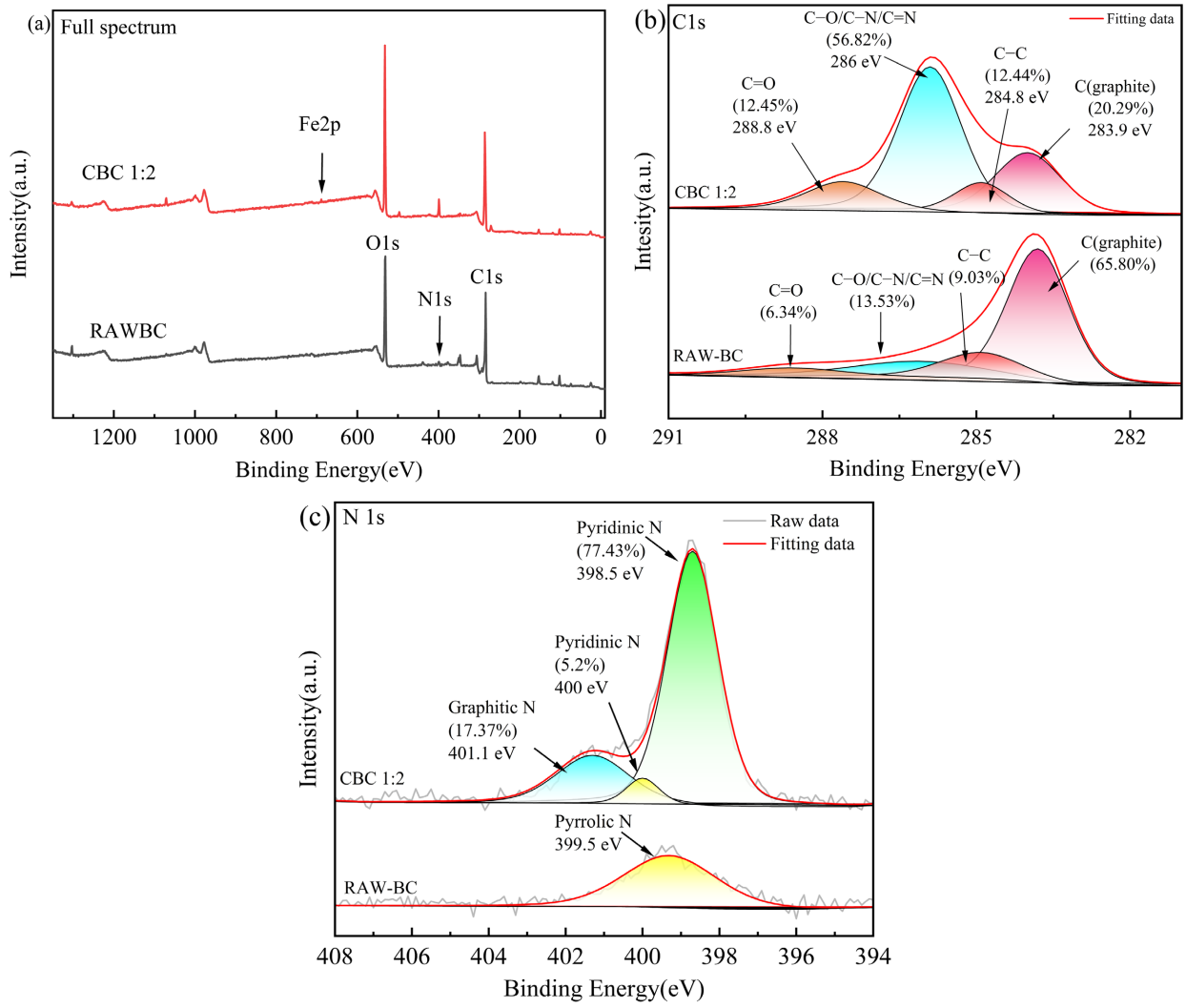

Figure 4. XPS spectral results of CBC and RAW-BC: (a) Full spectrum; (b) C1s spectrum; (c) N1s spectrum.

4.2. Adsorption Performance and Mechanistic Analysis of Biochar and Its Composites for Naphthalene in Soil and Aqueous Systems

The residual naphthalene concentration in the soil at 7, 14, 30, and 45 d under the condition of 10% addition is shown in Figure 5, and the naphthalene concentration in the soil decreased with time for each material. The residual concentration of RAW-BC was higher, and its adsorption capacity was small, while the advantage of CBC 1:2 was significant. Its residual concentration was already lower at 7 d and continued to decrease, with the removal rate at 45 d reaching 60.42%. The adsorption performance was enhanced by the pyridine nitrogen produced by the chitosan composite. Although the specific surface area of CBC 1:2 was slightly reduced (physical adsorption was weakened), more functional groups were introduced to enhance chemical adsorption, and thus the overall removal effect was more obvious (Oh et al., 2012).

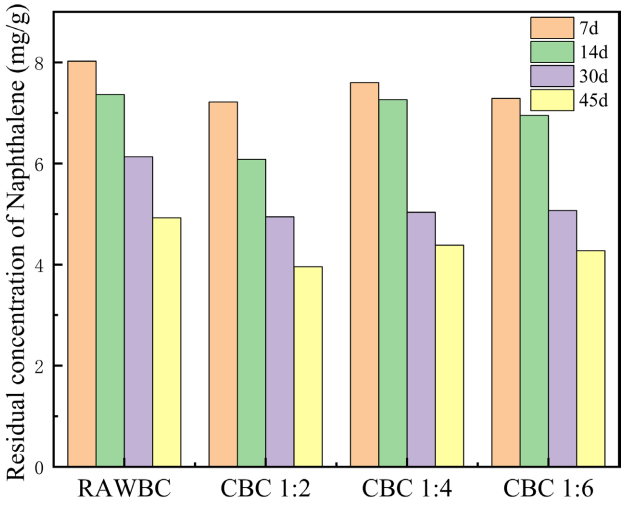

Figure 5. Adsorption of naphthalene in soil by biochar application.

During the period of 7 - 14 d, the changes in naphthalene adsorption by CBC 1:4, CBC 1:6, and RAW-BC were small. Physical adsorption was dominant at this stage, and the differences in the physical adsorption capacity of the three were insignificant, so the changes in the remaining naphthalene concentration were similar. From 14 - 30 d, the changes in adsorption by CBC 1:4 and CBC 1:6 were large, and the adsorption gradually transitioned to a synergistic effect between physical and chemical adsorption. Chemical adsorption was enhanced by the functional groups, such as pyridine nitrogen, generated by chitosan. As a result, the amount of naphthalene adsorbed by the former two increased significantly, and the remaining concentration decreased significantly, which was greater than that of RAW-BC.

To investigate the adsorption behavior of naphthalene in aqueous solution, kinetic adsorption experiments were conducted using a mixture of RAW-BC and CBC at a mass ratio of 1:2. According to the adsorption effect and the fitting results (see Table 1 and Figure 6), the experimental adsorption capacity of naph-

thalene by RAW-BC and CBC 1:2 was 22.13 mg/g and 31.99 mg/g, respectively. Rapid adsorption was achieved by both materials within 2 h, and the adsorption rate slowed down after 2 h until the adsorption equilibrium state was reached after 12 h. In the rapid adsorption stage, naphthalene was rapidly chemisorbed onto the outer surface of the biochar, when the adsorption capacity was the highest, and then naphthalene was gradually filled into the micropores of the internal pores through intra-particle diffusion (Sajjadi et al., 2019).

Table 1. Kinetic parameters of the adsorption of naphthalene by RAW-BC and CBC 1:2.

		Quasi-Primary Kinetic Model			Quasi-Secondary Kinetic Model			Elovich Model		
	$q_{e,exp}$ (mg/g)	$q_{e,cal}$ (mg/g)	$K_1/10^{-2}$ (min^{-1})	R^2	$q_{e,cal}$ (mg/g)	$K_2/10^{-2}$	R^2	lnα	β	R^2
RAW-BC	22.13	−5.5507	6.8626	−0.0644	22.463	0.5336	0.999 16	3.8513	0.1760	0.6631
CBC 1:2	31.99	6.8372	0.003 22	0.812 38	31.163	0.1396	0.999 85	2.3186	0.1630	0.8294

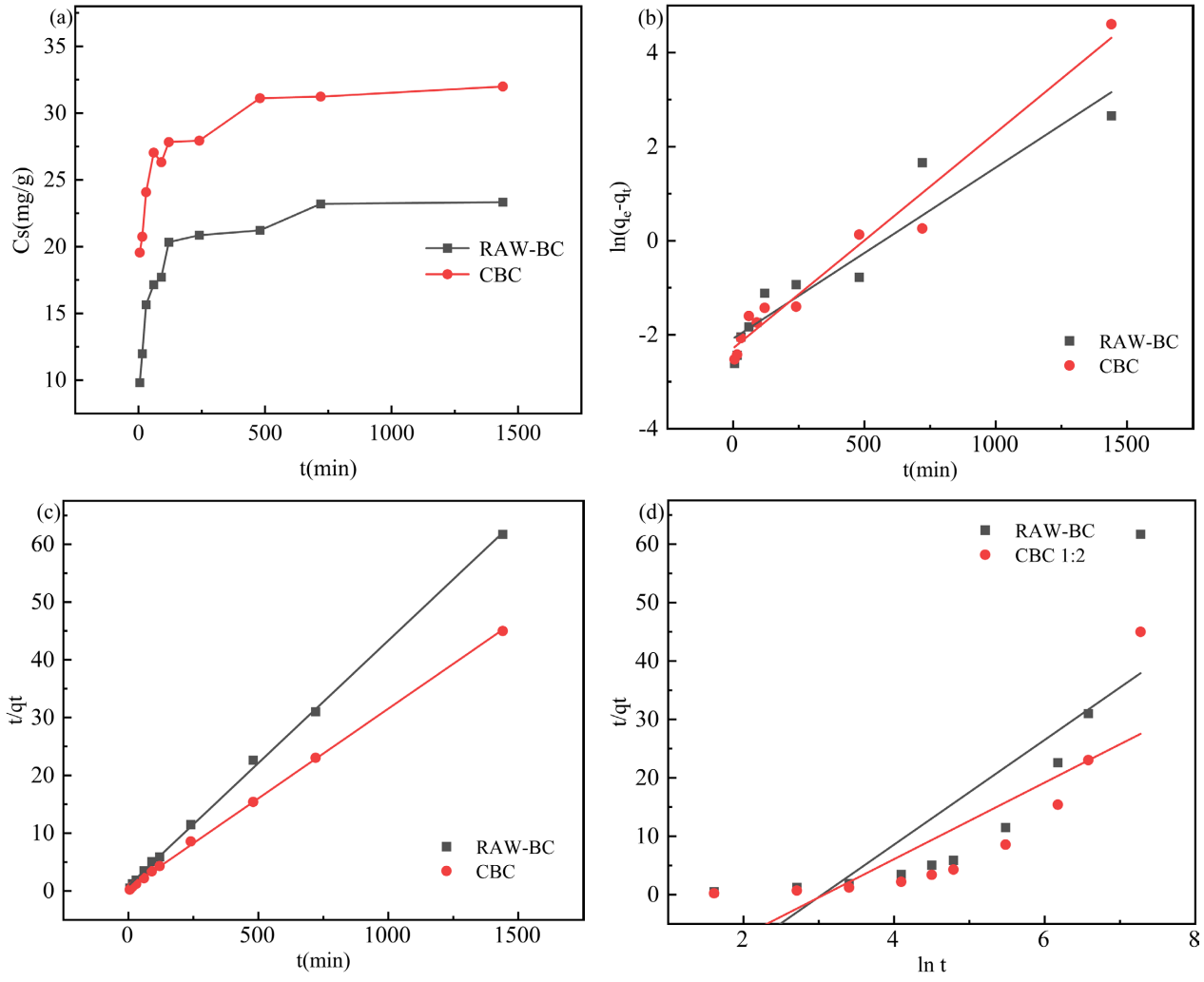

Figure 6. Kinetic results of adsorption of naphthalene by RAW-BC and CBC 1:2: (a) Adsorption results; (b) Quasi-first-order model fit; (c) Quasi-second-order model fit; (d) Elovich model fit.

5. Conclusion

The characterization of the CBC series showed that chitosan was successfully loaded on the surface and pores of the biochar, and the loading decreased with the decrease of chitosan proportion. Its oxygen-containing functional groups were enhanced, the specific surface area decreased, but the mesopore and the total pore volume increased, and XPS confirmed that the nitrogen content was increased, along with the formation of graphitic nitrogen and pyrrolizidine nitrogen structures, which are conducive to the adsorption of nonpolar polycyclic aromatic hydrocarbons (PAHs).

Funding

This study was partially supported by the National Natural Science Foundation of China (Grant No. 42271301).

Conflicts of Interest

The authors declare no conflicts of interest regarding the publication of this paper.

References

Ahmad, M., Lee, S. S., Dou, X., Mohan, D., Sung, J., Yang, J. E. et al. (2012). Effects of Pyrolysis Temperature on Soybean Stover- and Peanut Shell-Derived Biochar Properties and TCE Adsorption in Water. *Bioresource Technology, 118,* 536-544. https://doi.org/10.1016/j.biortech.2012.05.042

Akyüz, M., & Çabuk, H. (2010). Gas-Particle Partitioning and Seasonal Variation of Polycyclic Aromatic Hydrocarbons in the Atmosphere of Zonguldak, Türkiye. *Science of the Total Environment, 408,* 5550-5558. https://doi.org/10.1016/j.scitotenv.2010.07.063

Bronner, G., & Goss, K. (2011). Sorption of Organic Chemicals to Soil Organic Matter: Influence of Soil Variability and pH Dependence. *Environmental Science & Technology, 45,* 1307-1312. https://doi.org/10.1021/es102576e

Buttersack, C. (2019). Modeling of Type IV and V Sigmoidal Adsorption Isotherms. *Physical Chemistry Chemical Physics, 21,* 5614-5626. https://doi.org/10.1039/c8cp07751g

Cabrerizo, A., Dachs, J., & Barceló, D. (2009). Development of a Soil Fugacity Sampler for Determination of Air-Soil Partitioning of Persistent Organic Pollutants under Field Controlled Conditions. *Environmental Science & Technology, 43,* 8257-8263. https://doi.org/10.1021/es9020525

Chen, Z., Chen, B., & Chiou, C. T. (2012). Fast and Slow Rates of Naphthalene Sorption to Biochars Produced at Different Temperatures. *Environmental Science & Technology, 46,* 11104-11111. https://doi.org/10.1021/es302345e

Cheng, T., Li, J., Ma, X., Zhou, L., Wu, H., & Yang, L. (2022). Alkylation Modified Pistachio Shell-Based Biochar to Promote the Adsorption of VOCs in High Humidity Environment. *Environmental Pollution, 295,* Article ID: 118714. https://doi.org/10.1016/j.envpol.2021.118714

Ding, Y., Liu, Y., Liu, S., Li, Z., Tan, X., Huang, X. et al. (2016). Biochar to Improve Soil Fertility. A Review. *Agronomy for Sustainable Development, 36,* Article No. 36. https://doi.org/10.1007/s13593-016-0372-z

Du, W., Liu, M., Li, Y., Zhu, J., Wei, X., Yang, J. et al. (2021). Cross-Interface Transfer of Polycyclic Aromatic Hydrocarbons (PAHs) in a Shallow Urban Lake in Shanghai, China

Based on the Fugacity Model. *Science of the Total Environment, 736,* Article ID: 139369. https://doi.org/10.1016/j.scitotenv.2020.139369

Fabbri, D., Rombolà, A. G., Torri, C., & Spokas, K. A. (2013). Determination of Polycyclic Aromatic Hydrocarbons in Biochar and Biochar Amended Soil. *Journal of Analytical and Applied Pyrolysis, 103,* 60-67. https://doi.org/10.1016/j.jaap.2012.10.003

Fendinger, N. J., & Glotfelty, D. E. (1990). Henry's Law Constants for Selected Pesticides, PAHs and PCBs. *Environmental Toxicology and Chemistry, 9,* 731-735. https://doi.org/10.1002/etc.5620090606

Fu, H., Zhao, P., Xu, S., Cheng, G., Li, Z., Li, Y. et al. (2019). Fabrication of Fe_3O_4 and Graphitized Porous Biochar Composites for Activating Peroxymonosulfate to Degrade P-Hydroxybenzoic Acid: Insights on the Mechanism. *Chemical Engineering Journal, 375,* Article ID: 121980. https://doi.org/10.1016/j.cej.2019.121980

Gai, X., Wang, H., Liu, J., Zhai, L., Liu, S., Ren, T. et al. (2014). Effects of Feedstock and Pyrolysis Temperature on Biochar Adsorption of Ammonium and Nitrate. *PLOS ONE, 9,* e113888. https://doi.org/10.1371/journal.pone.0113888

Huang, P., Zhang, P., Wang, C., Tang, J., & Sun, H. (2022). Enhancement of Persulfate Activation by Fe-Biochar Composites: Synergism of Fe and N-Doped Biochar. *Applied Catalysis B: Environmental, 303,* Article ID: 120926. https://doi.org/10.1016/j.apcatb.2021.120926

Huang, Y., Lee, X., Grattieri, M., Yuan, M., Cai, R., Macazo, F. C. et al. (2020). Modified Biochar for Phosphate Adsorption in Environmentally Relevant Conditions. *Chemical Engineering Journal, 380,* Article ID: 122375. https://doi.org/10.1016/j.cej.2019.122375

Jones, K. C., & de Voogt, P. (1999). Persistent Organic Pollutants (POPs): State of the Science. *Environmental Pollution, 100,* 209-221. https://doi.org/10.1016/s0269-7491(99)00098-6

Kim, K., Jahan, S. A., Kabir, E., & Brown, R. J. C. (2013). A Review of Airborne Polycyclic Aromatic Hydrocarbons (PAHs) and Their Human Health Effects. *Environment International, 60,* 71-80. https://doi.org/10.1016/j.envint.2013.07.019

Kwapinski, W., Byrne, C. M. P., Kryachko, E., Wolfram, P., Adley, C., Leahy, J. J. et al. (2011). Biochar from Biomass and Waste. *Waste and Biomass Valorization, 1,* 177-189. https://doi.org/10.1007/s12649-010-9024-8

Kwon, G., Bhatnagar, A., Wang, H., Kwon, E. E., & Song, H. (2022). A Review of Recent Advancements in Utilization of Biomass and Industrial Wastes into Engineered Biochar. *Journal of Hazardous Materials, 400,* Article ID: 123242. https://doi.org/10.1016/j.jhazmat.2020.123242

Lee, J. E., & Park, Y. (2020). Applications of Modified Biochar-Based Materials for the Removal of Environment Pollutants: A Mini Review. *Sustainability, 12,* Article No. 6112. https://doi.org/10.3390/su12156112

Li, B., Liu, D., Lin, D., Xie, X., Wang, S., Xu, H. et al. (2020). Changes in Biochar Functional Groups and Its Reactivity after Volatile-Char Interactions during Biomass Pyrolysis. *Energy & Fuels, 34,* 14291-14299. https://doi.org/10.1021/acs.energyfuels.0c03243

Li, C., Xie, S., Wang, Y., Jiang, R., Wang, X., Lv, N. et al. (2021). Multi-Functional Biochar Preparation and Heavy Metal Immobilization by Co-Pyrolysis of Livestock Feces and Biomass Waste. *Waste Management, 134,* 241-250. https://doi.org/10.1016/j.wasman.2021.08.023

Li, R., Feng, C., Wang, D., Li, B., Hu, L., & Shen, Z. (2016). Role of Salinity in the Multiphase Redistribution of Polycyclic Aromatic Hydrocarbons (PAHs) in Sediment Suspension. *Environmental Earth Sciences, 75,* Article No. 116. https://doi.org/10.1007/s12665-015-5014-2

Li, Y., & Duan, X. (2015). Polycyclic Aromatic Hydrocarbons in Sediments of China Sea. *Environmental Science and Pollution Research, 22,* 15432-15442. https://doi.org/10.1007/s11356-015-5333-6

Luo, M., Lin, H., Li, B., Dong, Y., He, Y., & Wang, L. (2018). A Novel Modification of Lignin on Corncob-Based Biochar to Enhance Removal of Cadmium from Water. *Bioresource Technology, 259,* 312-318. https://doi.org/10.1016/j.biortech.2018.03.075

Mosleh, M. H., & Rajabi, H. (2024). NaOH-Benzoic Acid Modified Biochar for Enhanced Removal of Aromatic VOCs. *Separation and Purification Technology, 330,* Article ID: 125453. https://doi.org/10.1016/j.seppur.2023.125453

Oh, T. K., Choi, B. S., & Shinogi, Y. (2012). Characterization of Biochar Derived from Three Types of Biomass. *Journal of the Faculty of Agriculture, 57,* 61-66.

Queiroz, R. N., da Silva, M. G. C., Mastelaro, V. R., Prediger, P., & Vieira, M. G. A. (2023). Adsorption of Naphthalene Polycyclic Aromatic Hydrocarbon from Wastewater by a Green Magnetic Composite Based on Chitosan and Graphene Oxide. *Environmental Science and Pollution Research, 30,* 27603-27621. https://doi.org/10.1007/s11356-022-24198-9

Sajjadi, B., Broome, J. W., Chen, W. Y., Mattern, D. L., Egiebor, N. O., Hammer, N. et al. (2019). Urea Functionalization of Ultrasound-Treated Biochar: A Feasible Strategy for Enhancing Heavy Metal Adsorption Capacity. *Ultrasonics Sonochemistry, 51,* 20-30. https://doi.org/10.1016/j.ultsonch.2018.09.015

Shang, J., Chen, J., Shen, Z., Xiao, X., Yang, H., Wang, Y. et al. (2015). Photochemical Degradation of PAHs in Estuarine Surface Water: Effects of DOM, Salinity, and Suspended Particulate Matter. *Environmental Science and Pollution Research, 22,* 12374-12383. https://doi.org/10.1007/s11356-015-4543-2

Sun, K., Song, Y., He, F., Jing, M., Tang, J., & Liu, R. (2021). A Review of Human and Animals Exposure to Polycyclic Aromatic Hydrocarbons: Health Risk and Adverse Effects, Photo-Induced Toxicity and Regulating Effect of Microplastics. *Science of the Total Environment, 773,* Article ID: 145403. https://doi.org/10.1016/j.scitotenv.2021.145403

Sweetman, A. J., Valle, M. D., Prevedouros, K., & Jones, K. C. (2005). The Role of Soil Organic Carbon in the Global Cycling of Persistent Organic Pollutants (POPs): Interpreting and Modelling Field Data. *Chemosphere, 60,* 959-972. https://doi.org/10.1016/j.chemosphere.2004.12.074

Tremblay, L., Kohl, S. D., & Rice, J. A. (2005). Effects of Temperature, Salinity, and Dissolved Humic Substances on the Sorption of Polycyclic Aromatic Hydrocarbons to Estuarine Particles. *Marine Chemistry, 96,* 21-34.

Wang, D., Alaee, M., Byer, J., Liu, Y., & Tian, C. (2011). Fugacity Approach to Evaluate the Sediment-Water Diffusion of Polycyclic Aromatic Hydrocarbons. *Journal of Environmental Monitoring, 13,* 1589-1596. https://doi.org/10.1039/c0em00731e

Wang, J., & Guo, X. (2020). Adsorption Kinetic Models: Physical Meanings, Applications, and Solving Methods. *Journal of Hazardous Materials, 390,* Article 122156.

Wang, J., & Wang, S. (2019). Preparation, Modification and Environmental Application of Biochar: A Review. *Journal of Cleaner Production, 227,* 1002-1022. https://doi.org/10.1016/j.jclepro.2019.04.282

Wang, X., Guo, Q., Wang, X., Jia, Y., Chen, W., Zhang, Q. et al. (2023). Study on the Effects of New Developed Biochar and Sludge Composite Materials on Copper and Lead Contaminated Soil and Its Remediation Mechanism. *Environmental Technology & Innovation, 32,* Article ID: 103429. https://doi.org/10.1016/j.eti.2023.103429

Weissmann, M., Baranton, S., Clacens, J., & Coutanceau, C. (2010). Modification of Hy-

drophobic/Hydrophilic Properties of Vulcan XC72 Carbon Powder by Grafting of Trifluoromethylphenyl and Phenylsulfonic Acid Groups. *Carbon, 48,* 2755-2764. https://doi.org/10.1016/j.carbon.2010.04.003

Yuan, Z., Liu, G., Wang, R., & Da, C. (2014). Polycyclic Aromatic Hydrocarbons in Sediments from the Old Yellow River Estuary, China: Occurrence, Sources, Characterization and Correlation with the Relocation History of the Yellow River. *Ecotoxicology and Environmental Safety, 109,* 169-176. https://doi.org/10.1016/j.ecoenv.2014.08.024

Zhang, R., Zeng, L., Wang, F., Li, X., & Li, Z. (2022). Influence of Pore Volume and Surface Area on Benzene Adsorption Capacity of Activated Carbons in Indoor Environments. *Building and Environment, 216,* Article ID: 109011. https://doi.org/10.1016/j.buildenv.2022.109011

Zhang, Z., Wang, G., Li, W., Zhang, L., Chen, T., & Ding, L. (2020). Degradation of Methyl Orange through Hydroxyl Radical Generated by Optically Excited Biochar: Performance and Mechanism. *Colloids and Surfaces A: Physicochemical and Engineering Aspects, 601,* Article ID: 125034.

Zhu, H., Cheng, P., Zhong, B., & Wang, D. (2014). The Mechanisms of Contaminants Release Due to Incipient Motion at Sediment-Water Interface. *Science China Physics, Mechanics & Astronomy, 57,* 1563-1568. https://doi.org/10.1007/s11433-013-5255-6